

On the fatigue behavior of support structures for offshore wind turbines

N. Alati^{1a}, V. Nava^{2b}, G. Failla^{*1}, F. Arena^{1c} and A. Santini^{1d}

¹Department of Civil, Energy, Environmental and Materials Engineering (DICEAM),
University "Mediterranea" of Reggio Calabria, 89122 Reggio Calabria, Italy

²Tecnalia Research and Innovation, Parque Científico y Tecnológico de Bizkaia,
C/ Geldo. Edificio 700, E-48160 Derio (Bizkaia)

(Received November 22, 2012, Revised September 27, 2013, Accepted October 4, 2013)

Abstract. It is believed that offshore wind farms may satisfy an increasing portion of the energy demand in the next years. This paper presents a comparative study of the fatigue performances of tripod and jacket steel support structures for offshore wind turbines in waters of intermediate depth (20-50 m). A reference site at a water depth of 45 m in the North Atlantic Ocean is considered. The tripod and jacket support structures are conceived according to typical current design. The fatigue behavior is assessed in the time domain under combined stochastic wind and wave loading and the results are compared in terms of a lifetime damage equivalent load.

Keywords: offshore wind turbine; support structure; tripod; jacket; fatigue analysis

1. Introduction

A fatigue damage assessment is critical in the design of offshore wind energy converters (OWECs) (Hansen 2008, Manwell *et al.* 2010, Dong *et al.* 2011, 2012). In principle the driving dynamic excitations for fatigue, i.e., wind and waves, should be considered in a fully integrated nonlinear time domain simulation, where the aerodynamic and hydrodynamic loadings are generated simultaneously, in order to account for the coupling between aerodynamic and hydrodynamic responses, and various sources of nonlinearity are included (Kuhn 2001). This approach, however, involves as a major drawback a high computational effort, which is hardly compatible with the iterative nature of the design process when different, potential structural solutions shall be compared.

The research effort made, in the last decade, to develop more efficient but still reliable methods for fatigue analysis, has now led to a certain consensus on the following concepts (Kuhn 2001):

*Corresponding author, Researcher, E-mail: giuseppe.failla@unirc.it

^a Ph. D. Student, E-mail: natale.alati@unirc.it

^b Doctor of Philosophy, E-mail: vincenzo.nava@tecnalia.com

^c Full Professor, E-mail: arena@unirc.it

^d Full Professor, E-mail: adolfo.santini@unirc.it

- wind and wind-induced wave loadings can be regarded as independent and stationary processes on a short time scale, within a period of ten minutes to three hours; this is the typical time length of a time domain simulation for fatigue analysis;
- nonlinear constitutive relations and geometric nonlinearities do not play a significant role for fatigue response;
- the magnitude of the stress ranges in the soil due to wind or wave fatigue loading is small compared to the ultimate strength; thus the soil behavior can be assumed to be linear, and separate analyses of the aerodynamic and hydrodynamic responses with the same soil model are feasible.

On this theoretical basis, Kuhn (2001) and Van der Tempel (Van der Tempel and Molenaar 2002, Van der Tempel 2006) have recently proposed some simplified methods for fatigue analysis, in time and frequency domain. The key idea is that aerodynamic and hydrodynamic loadings are generated separately and then applied on the structural model. To account for the coupling between aerodynamic and hydrodynamic responses, ignored when separately generating the aerodynamic and hydrodynamic loadings, an additional damping is introduced in the structural model, generally referred to as aerodynamic damping (Kuhn 2001, Van der Tempel 2006). These methods allow considerable computational advantages, because well-established methods of wind and offshore industry can be used to separately generate the aerodynamic and hydrodynamic loadings, and results have been found in a good agreement with experimental data (Kuhn 2001, Van der Tempel 2006). In recognition of the accuracy and the computational advantages involved, these methods have been awarded a growing attention in the design of OWECs (Camp *et al.* 2003, ISSC 2006, Zaaier 2009).

A simplified method of particular interest is that proposed by Van der Tempel (2006). The separate generation of aerodynamic and hydrodynamic loadings is performed as follows: the aerodynamic loading assuming that the tower top is fixed, i.e., ignoring the tower top oscillations due to wind and wave loadings; the hydrodynamic loading by Morison equation for fixed structures. These loadings are applied on a linear structural model where the aerodynamic damping is added in the fundamental fore-aft flexural mode. It is important to remark that, without introducing the aerodynamic damping when applying the separately generated aerodynamic and hydrodynamic loadings, the vibration response computed in the structural model (including tower, support structure and foundation) would be erroneously larger than the actual vibration response computed by a fully integrated time domain simulation, where the aerodynamic and hydrodynamic loadings are generated simultaneously. This result is well known in the literature and is attributed to the fact that the tower top oscillations due to wind and wave loadings, which are ignored when separately generating the aerodynamic loading under the assumption that the tower top is fixed, significantly affect the instantaneous thrust force, and produce indeed damping effects. In fact a tower top motion against or in the wind direction causes, respectively, an increase or a decrease of the instantaneous thrust force, with respect to that computed assuming that the tower top is fixed. The fact that, in both situations, this alternation of the thrust force is oriented opposite to the tower top motion, explains why its effects are generally modeled as damping effects (page 124 in the work by Van der Tempel (2006); see also page 104 in the work by Kuhn (2001)).

The method by Van der Tempel (2006), as applied to a typical OWEC under combined wind and wave loadings, has provided numerical results in excellent agreement with experimental data recorded in some offshore sites, and numerical results obtained by fully integrated nonlinear time domain simulations (Van der Tempel 2006). There are also some other considerable advantages. Being computed under the assumption that the tower top is fixed, the aerodynamic loading applies

regardless of the structural parameters of tower, support structure and foundation. This may appear particularly suitable for design purposes as in fact, to build the structural response for different geometric and/or mechanical parameters, straightforward linear analyses can be carried out by always using the same aerodynamic loading, without performing time-consuming nonlinear aero-elastic analyses. A further relevant advantage is that it is possible to introduce, in the structural model, a suitable model of soil-structure interaction. This is not generally feasible, instead, in the fully integrated nonlinear time domain simulations, as implemented in most commercial software.

The aim of this paper is to carry out a comparative fatigue analysis of two support structures for OWECs, a tripod and a jacket, both resting on a pile foundation. This subject is of particular interest since in waters deeper than 20 m, where to minimize the visual impact an increasing number of wind farms is planned in the future, tripods and jackets are generally preferred to monopiles, that would require too large diameters and masses. To date, however, no general consensus has been attained on whether the tripod or the jacket is the preferable option and extensive experimental tests are still ongoing on this matter (Homepage “Alpha Ventus”, Homepage “Beatrice Wind Farm”).

The comparative fatigue analysis is carried out in the time domain on two test structures, following the basic principles of the method by Van der Tempel (2006). The latter, in light of computational efficiency, reliability versus available experimental tests and possibility of soil-pile interaction modeling, appears as most suitable for the purposes of this paper. Therefore, stochastic aerodynamic and hydrodynamic loadings are generated separately and then applied on finite element (FE) models of the test structures, where additional aerodynamic damping is introduced. Fatigue performances are compared in terms of appropriate equivalent loads, which include different load cases with the related probabilities of occurrence.

The paper is organized as follows. The test structures are illustrated in Section 2. The generation of the aerodynamic and hydrodynamic loadings is described in Section 3. Fatigue analysis is outlined in Section 4. Numerical results are presented in Section 5. The structural details of the test structures are reported in the Appendix.

2. Structural models

A site in the North Atlantic Ocean, offshore the southern coast of Iceland (63°00' N, 20° 00' W), is considered as a reference site. Statistical data on the correlation between sea states (wave period, wave height) and mean wind velocity are available at the homepage www.windclimate.com. The design water depth is 45 m.

2.1 Tripod and jacket support structures

The turbine is the reference 5MW three-bladed turbine designed by the National Renewable Energy Laboratory (NREL). Blade geometry, power transmission and full details can be found in the NREL report by Jonkman *et al.* (2009). Two steel structures are considered, shown in Fig. 1. They are mounted on a center column tripod and a jacket quattropod respectively, both resting on pile foundations. For brevity, the test structure with the center column tripod will be referred to as CCT, and the test structure with the jacket quattropod as JQ.

For the CCT and the JQ, the following parameters are identical: hub height above the still water level (SWL), water depth (45 m), length and diameter of the piles, tower diameter. Dimensions of the structural members are designed according to current practice. Details on the geometry of the structural members and constructional steel parameters are given in the Appendix. The CCT and the JQ are designed to have almost the same natural frequency of the first fore-aft flexural mode in the wind direction, consistently with similar studies comparing structural performances of tripods and jackets (Subroto *et al.* 2006, Jonkman and Musial 2010, Song *et al.* 2012, Song *et al.* 2013, De Vries 2011). This choice is made in recognition of the fact that the natural frequency of the first fore-aft flexural mode is a typical design parameter, which is generally selected depending on the frequency range of the excitation and regardless of the specific support structure to be adopted.

The FE models of the two structures are built in SAP2000 (Computers and Structures 2010) by using 3D beam elements with shear deformation. In the FE models a total lumped mass is considered at the tower top, which includes the mass of the rotor and nacelle assembly (RNA). This lumped mass is equal to $3.4 \cdot 10^5$ kg. For the stress resultants in the tower, the positive sign conventions are reported in Fig. 1. The same conventions hold for the stress resultants in the foundation piles.

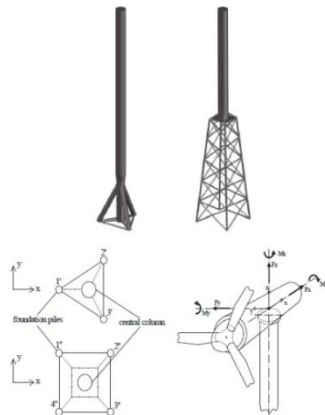


Fig. 1 Test structures: pile foundations and stress resultants in JQ and CCT

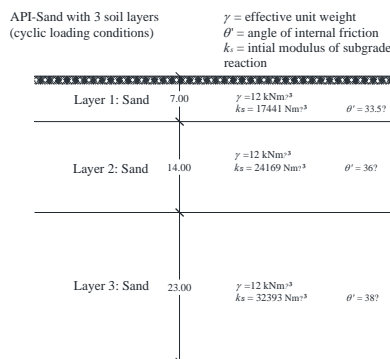


Fig. 2 Reference soil layers

2.2 Foundation modeling

The reference soil characteristics are reported in Fig. 2. Pile-soil interaction is modeled by lateral and vertical springs distributed along the length of the pile, with a vertical spring located at the pile tip (Al Hamaydeh and Hussain 2011, Zaaier 2006). All springs are supposed to be uncoupled. In principle, the constitutive law of the springs should be taken as nonlinear, based on the p - y relation (p = load per unit length; y = deflection) provided by the API code (API 2000). However, in view of the expected low stress range induced by operational loads, the tangent stiffness at $y = 0$ can be assumed for the stiffness of the linear springs (Kuhn 2001).

2.3 Modal analysis

Table 1 reports the natural frequencies of the first 4 vibration flexural modes, the stiffness of the two structures for each stress direction in Fig. 1 (K_{Fx} , K_{Fy} , K_{Fz} = translational stiffness; K_{Mx} , K_{My} , K_{Mz} = rotational stiffness), and the total masses. It can be seen that the CCT is stiffer than the JQ, for all stress directions. The total mass of the CCT ($M_{CCT} = 4.36 \cdot 10^6$ kg) is larger than the mass of the JQ ($M_{JQ} = 2.99 \cdot 10^6$ kg).

The two structures exhibit almost the same natural frequency of the first fore-aft flexural mode, which occurs in the x -direction. Although mass and stiffness distributions are obviously different in the two structures, this result is not surprising since the CCT has a larger total mass but also a greater stiffness in the x -direction, as shown in Table 1. Examples of CCTs and JQs with almost the same natural frequency of the first fore-aft flexural mode can be found in many other comparative studies on OWECs with tripod and jackets (Subroto *et al.* 2006, Jonkman and Musial 2010, Song *et al.* 2012, Song *et al.* 2013, De Vries 2011). Frequency and stiffness values reported in Table 1 are in the typical range of current design (Subroto *et al.* 2006, Jonkman and Musial 2010, Song *et al.* 2012, Song *et al.* 2013, De Vries 2011).

Table 1 Natural frequencies and stiffness of the two test structures for the six stress directions in Fig. 1, and total mass

N. mode	Mode	JQ [Hz]	CCT [Hz]
1	1 st fore-aft	0.2050	0.2179
2	1 st side-side	0.2050	0.2179
3	2 nd fore-aft	1.1454	1.5032
4	2 nd side-side	1.1454	1.5032
Stiffness		JQ	CCT
K_{Fx} [Nm^{-1}]		$2.36 \cdot 10^6$	$3.47 \cdot 10^6$
K_{Fy} [Nm^{-1}]		$2.36 \cdot 10^6$	$3.47 \cdot 10^6$
K_{Fz} [Nm^{-1}]		$5.37 \cdot 10^8$	$3.90 \cdot 10^9$
K_{Mx} [Nm]		$1.00 \cdot 10^{10}$	$2.06 \cdot 10^{10}$
K_{My} [Nm]		$1.00 \cdot 10^{10}$	$2.06 \cdot 10^{10}$
K_{Mz} [Nm]		$7.2 \cdot 10^8$	$8.06 \cdot 10^9$
Total mass		JQ [kg]	CCT [kg]
		$2.99 \cdot 10^6$	$4.36 \cdot 10^6$

3. Aerodynamic and hydrodynamic loading

For fatigue analysis purposes, the response to combined stochastic wind and wave loadings is computed by a time domain Monte Carlo simulation. Following the key idea of the method by Van der Tempel (2006), the aerodynamic and hydrodynamic loadings are generated separately and then applied on the FE models of the two structures, where the additional aerodynamic damping is introduced. It is assumed that wind and waves act in the x direction (see Fig. 1). Note that collinear and unidirectional waves generally results in conservative fatigue loads, with respect to circumstances where a misalignment between wind and wave direction is considered (Kuhn 2001).

The aerodynamic loading at the tower top is generated assuming that the tower top is fixed, using the BLADED onshore wind turbine design tool (Garrad and Partners 2009). As customary, the turbulent part of the wind process is modeled as a zero mean Gaussian stationary process, a realization of which can be cast in the form (Shinozuka and Deodatis 1988)

$$w(t) = \sum_{j=1}^{K_w} \sqrt{2S_w(f_j) \Delta f_j} \cos(2\pi f_j t + \varphi_j) \quad (1)$$

where Δf_j is a constant step on the frequency axis, K_w is the number of frequency steps, $f_j = j\Delta f_j$ for $j=1,2,\dots,K_w$, φ_j 's are independent random phases uniformly distributed on $[0,2\pi]$ and $S_w(f)$ is the von Karman one-sided power spectral density (PSD)

$$S_w(f) = \frac{4\sigma_w^2 L_w/V_w}{\left[1 + 70.8(f L_w/V_w)^2\right]^{5/6}} \quad (2)$$

In Eq. (2) f is the frequency, V_w and σ_w are mean and standard deviation of the wind velocity, L_w is the integral length scale. These parameters in Eq. (2) are site depending and, for fatigue analysis purposes, they will be set in Section 4. In general, the wind loading causes six stress resultants at the tower top (see the sign conventions in Fig. 1).

For both structures, the hydrodynamic loading is built based on the slender body theory, adopting the definition by Chakrabarti (1987), with the wave kinematics calculated in an undisturbed wave field. This approximation is valid for values of the Keulegan-Carpenter number greater than 1 (Brebbia and Walker 1979, Sarpkaya and Isaacson 1981). Following a well-established literature concerning the computation of wave forces acting on slender bodies (Chakrabarti 1987, Di Paola and Failla 2002, Elshafey *et al.* 2009, Dong *et al.* 2011, 2012) and on support structures for OWECs in particular (Kuhn 2001, Van der Tempel 2006), the hydrodynamic loading is built by Morison equation for fixed structures. This is a widely accepted approximation in the analysis of offshore OWECs, in consideration of the rigidity of the support structures involved (see page 100 and page 199 of the work by Kuhn (2001); page 23 of the work by Van der Tempel (2006)), and is also consistent with recommended design practice (DNV-RP-C205 2010). Using Morison equation for fixed structures, the hydrodynamic loading is obtained as the sum of the following drag and inertia forces, which involve the absolute velocities and accelerations of the water particles

$$f_{Morison}(x, z, t) = f_d(x, z, t) + f_i(x, z, t); \quad (3)$$

$$f_d(x, z, t) = C_d \cdot \frac{1}{2} \rho_{water} D \cdot |u(x, z, t)| u(x, z, t); \quad (4)$$

$$f_i(x, z, t) = C_m \frac{\rho_{water} \pi D^2}{4} a(x, z, t), \quad (5)$$

where D is the diameter of the generic cylindrical structural member, C_d is the hydrodynamic drag coefficient, C_m is the hydrodynamic inertia coefficient (Boccotti *et al.* 2012, 2013), ρ_{water} is the water density, $u(x, z, t)$ and $a(x, z, t)$ are the absolute velocity and acceleration of the water particle, for which horizontal (u_x and a_x) and vertical components (u_z and a_z) are considered. In general, the hydrodynamic coefficients C_d and C_m can be determined as functions of the dimensionless Reynolds and Keulegan-Carpenter numbers (Sarpkaya and Isaacson 1981). In this work $C_d = 0.62$ and $C_m = 1.85$ have been assumed, i.e., the asymptotic values for these coefficients, which can be found for a ratio of the Reynolds number to the Keulegan number larger than 10000. The water density has been set as $\rho_{water} = 1030 \text{ kgm}^{-3}$.

According to the sea states theory for an irrotational wave motion (Philips 1967, Longuet-Higgins 1963), the free surface displacement can be considered as the following summation of elementary components

$$\eta(x, t) = \sum_{j=1}^{K_\eta} \sqrt{2S_{JS}(f_j) \Delta f_j} \cos(k_j x - 2\pi f_j t + \psi_j) \quad (6)$$

where, as in Eq. (1), Δf_j is a constant step on the frequency axis, K_η is the number of frequency steps, $f_j = j \Delta f_j$ for $j=1, 2, \dots, K_\eta$, ψ_j 's are independent random phases uniformly distributed on $[0, 2\pi]$. Further

$$k_j \tanh(k_j d) = \frac{(2\pi f_j)^2}{g}, \quad (7)$$

where d denotes the water depth, k_j the wave number, g the gravity acceleration, and $S_{JS}(f)$ is the JONSWAP one-sided PSD (Hasselmann *et al.* 1973) given as

$$S_{JS}(f) = \alpha g^2 (2\pi f)^{-5} \exp\left[-\frac{5}{4} \left(\frac{f_p}{f}\right)^4\right] \cdot \exp\left\{\ln \gamma \exp\left[-\frac{(f-f_p)^2}{2\sigma^2 f_p^2}\right]\right\} \quad (8)$$

In Eq. (8) f_p is the peak spectral frequency, α is Phillips' parameter taken as $\alpha = 0.01$, while the parameters characterizing the mean JONSWAP spectrum are

$$\gamma = 3.3 \quad \sigma \begin{cases} = 0.07 & \text{if } f \leq f_p \\ = 0.09 & \text{if } f > f_p \end{cases} \quad (9)$$

Under the assumption of irrotational wave motion, the potential of velocity function can be determined as

$$\phi(x, z, t) = \sum_{j=1}^{K_\eta} \sqrt{2S_{JS,potential}(f_j, z) \Delta f_j} \cdot \sin(k_j x - 2\pi f_j t + \psi_j) \quad (10)$$

where

$$S_{JS,potential}(f_j, z) = g [k_j \tanh(k_j d)]^{-1} S_{JS}(f_j) \left\{ \frac{\cosh[k_j(d+z)]}{\cosh(k_j d)} \right\}^2 \quad (11)$$

Using Eq. (10), the horizontal and vertical components of the water particles velocity and acceleration in Eqs. (4) and (5) can be computed as

$$u_x = \partial\phi/\partial x ; u_z = \partial\phi/\partial z ; \quad (12a,b)$$

$$a_x = \partial^2\phi/\partial x\partial t ; a_z = \partial^2\phi/\partial z\partial t . \quad (12c,d)$$

The Monte-Carlo simulation is implemented based on the Fast Fourier Transform (Spanos and Zeldin 1998). The sampling frequency is selected in order to ensure Gaussianity and ergodicity of the simulated stochastic wind and wave processes. The aerodynamic loading at the tower top, as computed by BLADED onshore tool (Garrad and Partners 2009) upon introducing the simulated wind loading, along with the hydrodynamic loading given by Eqs. (3)-(5), built based on the simulated free surface displacement (6) and potential (10), are applied on the FE models of the two structures, where the additional aerodynamic damping introduced in the fundamental fore-aft flexural mode is set equal to 4%. This is a satisfactory engineering estimate for fatigue analysis purposes (Van der Tempel 2006).

4. Fatigue analysis

Fatigue damage analysis is carried out within the framework of the Miner-Palmgren theory (Sutherland 1999). Denoting by N the maximum number of stress cycles that a material can withstand under a stress range S , it yields

$$N = k \cdot S^{-m}, \quad (13)$$

where m is the Wöhler integer exponent depending on the material and k is a structure depending parameter. For constructional steel, $m = 4$ is generally set (Sutherland 1999, Thomsen 1998). Given the number of cycles n_i , which the material is subjected to at a given stress range S_i , a total damage index D_T can be evaluated by linear superposition of the damage indexes d_i associated with each stress range S_i , according to the Miner-Palmgren law

$$d_i = \frac{n_i}{N_i}; D_T = \sum_i d_i = \sum_i \frac{n_i}{N_i} \quad (14)$$

A damage equivalent stress S_{eq} can be defined as the mean stress that would produce, in an equivalent number of cycles n_{eq} , the same amount of damage produced by the actual individual stress ranges, according to the equivalence formula

$$D = \sum_i \frac{n_i}{N_i} = \sum_i \frac{n_i}{k} S_i^m = \frac{n_{eq}}{k} S_{eq}^m \Rightarrow S_{eq} = \sqrt[m]{\frac{k}{n_{eq}} \sum_i \frac{n_i}{k} S_i^m} = \sqrt[m]{\sum_i \frac{n_i}{n_{eq}} S_i^m} \quad (15)$$

In Eq. (15), n_{eq} is conventionally chosen as $n_{eq} = f_{eq} \cdot T_{eq}$, where $f_{eq} = 1$ and T_{eq} is equal to the

time series length.

Therefore, for all the stress resultants such as normal and shear forces, bending and twisting moments shown in Fig. 1, a damage equivalent load (DEL) can be defined as Eq. (15), and a lifetime damage equivalent load ($DEL_{lifetime}$). The latter accounts for the fact that each load case is a stochastic load case that corresponds to a wind velocity class with a certain probability of occurrence, and is introduced as follows (Andersen 2008)

$$DEL_{lifetime} = \sum_{j=1}^M \sqrt[n_{eq,lifetime}]{\frac{1}{N_s} \sum_{l=1}^{N_s} \frac{DEL_l^m}{N_s} n_{eq} \cdot P_j \cdot n_t} \quad (16)$$

where M is the number of wind velocity classes V_{wj} ; P_j is the probability associated with each wind velocity class; N_s is the number of realizations generated for each load case; DEL_l is the damage equivalent load associated with each realization; n_t is the ratio of the total lifetime to the fatigue simulation time length; $n_{eq,lifetime}$ is the number of equivalent stress cycles in the lifetime, conventionally chosen as $n_{eq,lifetime} = f_{eq,lifetime} T_{eq,lifetime}$ where $f_{eq,lifetime} = 1$ and $T_{eq,lifetime}$ is the design lifetime, which for an OWEC is typically 20 years. To reduce the computational effort while preserving accuracy, in Eq. (16) a certain number of lumped load cases are considered, each defined by a certain wind velocity V_{wj} and a related probability of occurrence P_j . With a given wind velocity V_{wj} the following equivalent wave height H_{sj} and equivalent wave period T_{zj} are associated

$$H_{sj}^m \sum_{i=1}^{N_{Hj}} p_i = \sum_{i=1}^{N_{Hj}} p_i H_{sj,i}^m \Rightarrow H_{sj} = \sqrt[m]{\sum_{i=1}^{N_{Hj}} p_i H_{sj,i}^m / \sum_{i=1}^{N_{Hj}} p_i} \quad (17)$$

$$\frac{1}{T_{zj}} \sum_{i=1}^{M_{Tj}} p_i = \sum_{i=1}^{M_{Tj}} p_i \frac{1}{T_{zj,i}} \Rightarrow \frac{1}{T_{zj}} = \sum_{i=1}^{M_{Tj}} p_i \frac{1}{T_{zj,i}} / \sum_{i=1}^{M_{Tj}} p_i \quad (18)$$

where p_i are the probabilities ($0 < p_i < 1$) of the various environmental states ($H_{sj,i}$; $T_{zj,i}$) included in the lumped load case defined by the wind velocity V_{wj} , such that $\sum p_i = P_j$, being P_j the

probability of occurrence related to the wind velocity class V_{wj} . Also, N_{Hj} and M_{Tj} denote the number of wave height and wave period bins included in the lumped load case defined by the wind velocity class V_{wj} . All these data are site depending (for the reference site of this study, they are available at the homepage www.vaveclimate.com). As a result of Eqs. (17) and (18), the lumped load cases defined by the wind velocity classes V_{wj} , along with the related probabilities P_j to be used in Eq. (16), are reported in Table 2 (indexes j are omitted for brevity).

Fatigue caused by the production load cases is considered (parked or transitional behavior would require, in general, a different modeling of the aerodynamic damping, for this see the work by Kuhn (2001)). For each lumped load case in Table 2, 100 couples of independent realizations of the aerodynamic and hydrodynamic loadings are generated as explained in Section 3. To generate the turbulent part of the wind, for each wind class the parameters in Table 2 are considered.

The rainflow counting algorithm is applied to determine stress ranges and corresponding number of cycles for fatigue damage analysis (Matsuiski and Endo 1969). Then the lifetime DEL

is computed based on Eq.(16) for each stress resultant.

Table 2 Lumped load cases and turbulent wind field parameters for different wind velocity classes in lifetime DEL, Eq. (16)

V_w [ms ⁻¹]	3	5	7	9	11	13	15	17	19	21
H_s [m]	2.94	3.36	3.54	3.83	4.26	4.93	5.84	6.34	7.53	9.27
T_z [s]	6.92	6.68	6.45	6.50	6.87	7.20	7.56	8.30	9.05	10.8
P (%)	6.4	12.2	16.9	17.9	16.1	12.3	7.8	4.6	2.1	1.0
Int. turb. %	2.88	4.94	5.80	6.34	6.75	7.08	7.36	7.60	7.81	8.00
L_w [m]	23.36	54.20	78.12	99.99	121.13	141.69	161.56	180.65	189.90	216.4
σ_w [ms ⁻¹]	0.087	0.247	0.406	0.570	0.742	0.920	1.104	1.292	1.484	1.680

5. Numerical results

The lifetime DEL is computed for wind loading only, i.e., for wind in a calm sea, and for wind + wave loading. Results are reported at the tower base and at the foundation level, corresponding to the top of the pile foundation (see sign conventions for the stress resultants in Fig. 1). In this respect, it is worth remarking that the DELs are not expected to be equal in the four piles of the JQ, as a result of the asymmetry due to the wind-induced M_z stress resultant at the tower top. Obviously the same can be stated for the three piles of the CCT. For this reason, in each structure the pile where the highest DELs are encountered will be chosen, for comparison at the foundation level.

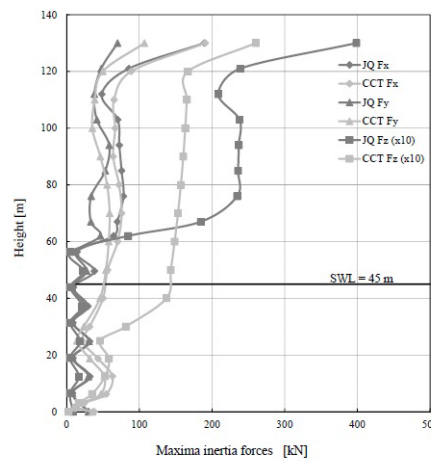
Prior to discuss the result of the fatigue analysis, a few remarks are worth doing on which structure will feature, in general, the largest inertia forces. In this respect, it shall be pointed out that the JQ and the CCT are designed to have almost the same natural frequencies of the first fore-aft flexural modes in the x- and y- directions but exhibit different stiffness and total mass. As shown in Table 1, the CCT is stiffer than the JQ, and the total mass of the CCT ($M_{CCT} = 4.36 \cdot 10^6$ kg) is larger than the total mass of the JQ ($M_{JQ} = 2.99 \cdot 10^6$ kg). Further, the mass distribution is different, since the tower mass + top mass is equal to 75.5% of the total mass in the CCT, while the tower mass + top mass is equal to 85% of the total mass in the JQ. Based on these considerations, it is evident that an *a priori* estimation of where the inertia forces shall be larger, i.e. in the CCT or in the JQ, is not feasible and that any conclusion in this respect shall be drawn from the time domain numerical simulations.

For this purpose, Fig. 3 shows the profile of the maxima inertia forces in the x-, y- and z-direction, due to the simulated wind loading corresponding to the most likely environmental state ($V_w = 9$ ms⁻¹) in Table 2, i.e., the most relevant one in the statistical determination of the lifetime DEL (16) for its relatively higher probability of occurrence. Specifically, the maxima inertia forces

in Fig. 3 are computed by averaging the maxima inertia forces obtained, for each realization of the wind loading, at the structural nodes corresponding to different heights on the two structures. The resultants of the inertia forces above the tower base and above the foundation level are also reported. Fig. 3 shows that in both structures the dynamic response is dominated by the first fore-aft flexural modes. The inertia forces in the x- and y- direction are larger in the CCT, while in the z- direction are larger in the JQ.

For the same environmental state ($V_w = 9 \text{ ms}^{-1}$) considered in Fig. 3, Fig. 4 shows the profile of the maxima inertia forces in the x-, y- and z- direction, due to wind + wave loading. It is seen that the total inertia forces in the x- direction increase significantly in the CCT, both at the tower base and at the foundation level, while less significant variations are found in the JQ. This result reflects that the total wave loading on the CCT is much larger, due to the larger diameters of the structural members involved and due to the fact that, unlike the JQ, the CCT features part of the tower under the still water level (structural details are in the Appendix). See in this respect Fig. 5, that shows the total wave loading due to a single realization of the wave process for the environmental state $V_w = 9 \text{ ms}^{-1}$. On the other hand, no variations are encountered in the inertia forces in the y-direction, as expected since the total wave loading has no component in the y-direction. Further, no significant variations are encountered in the inertia forces in the z-direction, both in the CCT and in the JQ. They appear almost the same as the corresponding resultants due to wind loading only, with slight differences in the related profiles.

The same conclusions can be drawn also for the other relevant environmental states in Table 2 and are not reported for brevity. In the next Sections it will be seen that the maxima inertia forces, as described above, provide a key to interpret the results in terms of DELs.



Inertia forces Fx	JQ	CCT
Tower base [kN]	754.16	831.12
Foundation [kN]	964.23	1088.24
Inertia forces Fy	JQ	CCT
Tower base [kN]	422.25	572.89
Foundation [kN]	609.42	787.37
Inertia forces Fz	JQ	CCT
Tower base [kN]	20599.17	17364.64
Foundation [kN]	21721.82	19601.53

Fig. 3 Maxima inertia forces in the x, y, z- direction due to wind loading for $V_w = 9 \text{ ms}^{-1}$ in Table 2

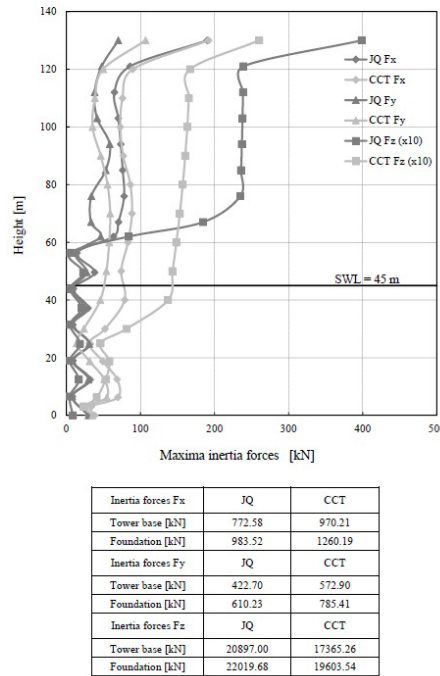


Fig. 4 Maxima inertia forces in the x, y, z- direction due to wind + wave loading for $V_w = 9 \text{ ms}^{-1}$ in Table 2

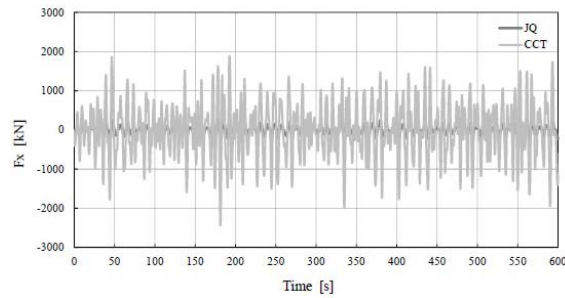


Fig. 5 Total wave loading in the x-direction

5.1 Aerodynamic loading in a calm sea

Fig. 6 shows the lifetime DELs at the tower base for wind loading only in a calm sea. In general, the DELs are higher in the CCT than in the JQ, except for the M_z DEL that is practically the same for the two structures. As far as the F_x , F_y , M_x , M_y DELs are concerned, it can be stated that they appear all consistent with the inertia forces shown in Fig. 3, whose resultants at the tower base are larger in the CCT than in the JQ. It shall be also pointed out that, although the inertia

forces in the z- direction are larger in the JQ than in the CCT, as shown in Fig. 3, the Fz DEL is larger in the CCT than in the JQ since the weight of the CCT tower is 1.45 times larger than the weight of the JQ tower (the weight of the RNA is equal for both structures). The Mz DEL is the same for the CCT and the JQ since, in both structures, the first torsional mode is a high frequency mode (5.35 Hz for the JQ and 9.64 Hz for the CCT). As a consequence, the response to Mz is a *pseudo*-static response where, for the tower equilibrium, the Mz stress at the tower base is obviously equal for both structures.

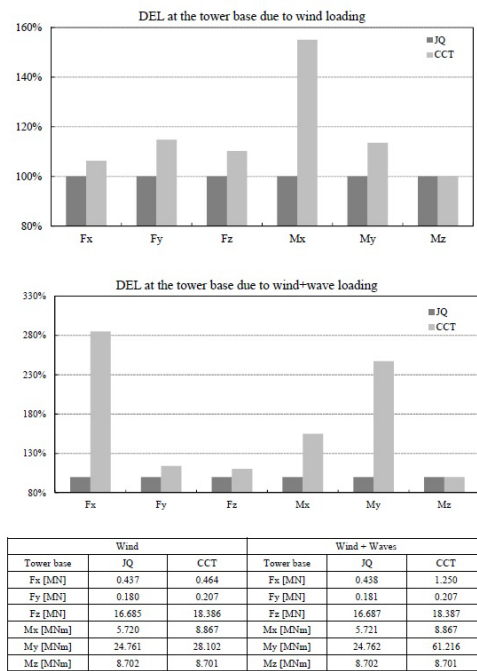


Fig. 6 Lifetime DEL at the tower base due to wind and wind + wave loading

Fig. 7 shows the lifetime DELs at the foundation level for wind loading only in a calm sea, for pile n. 1' of the CCT and pile n. 1" of the JQ. As a general comment, it can be pointed out that while at the tower base the highest DEL is due to bending effects (Mx and My, with Mx higher than My since the wind acts in the x- direction) and to axial effects (due to weight of the tower + RNA and the aerodynamics of the blades, Fz takes on significant values), at the foundation level the most significant DEL is due to Fz. This result is expected since, consistently with the design purposes of a tripod or a jacket support structure, the rotational equilibrium against the tilting effect induced by lateral loading (wind and/or waves) is provided by the Fz forces on the piles. A further relevant comment is that the Fz, Mx, My and Mz DELs appear consistent with the inertia forces shown in Fig. 3, larger in the CCT than in the JQ as shown by the resultants at the foundation level. On the other hand, the Fx and Fy DELs are found slightly larger in the JQ.

This result is essentially due to the fact that the Fx and Fy DELs in pile n. 1" of the JQ are significantly affected by the twisting effects due to Mz transmitted by the tower. See in this respect

Fig. 8, that shows the F_x and F_y DEL in pile n. 1' of the CCT and in pile n. 1'' of the JQ for M_z only acting at the tower top, due to wind loading.

5.2 Combined aerodynamic and hydrodynamic loading

Fig. 6 shows the lifetime DELs at the tower base for wind + wave loading. It can be stated that, as already encountered for wind loading only, the DELs are larger in the CCT than in the JQ. It is also seen that the F_x and M_y DELs are much larger in the CCT than in the JQ. This result can be attributed to the wave loading acting on the submerged part of the CCT tower (see Appendix for structural details) and, also, appears consistent with the fact that the maxima inertia forces in the x-direction due to wave loading increase (see Fig. 4), with respect to the corresponding ones due to wind loading only (see Fig. 3), much more in the CCT than in the JQ. It shall be pointed out that especially the increase in the M_y DEL of the CCT appears significant. On the other hand, for both structures no variations are found in the F_y and M_x DELs with respect to the corresponding DELs due wind loading only, as expected since the total wave loading has no components in the y-direction. In this regard, see also that the maxima inertia forces in the y-direction due to wind + wave loading (Fig. 4) and wind loading only (Fig. 3) are practically the same. Further, it is seen that the F_z DEL does not vary with respect to the F_z DEL due to wind loading only, consistently with the fact that no significant variations are encountered in the maxima inertia forces in the z-direction (see Figs. 3 and 4). Finally, no differences in terms of M_z DEL are encountered with respect to the M_z DEL due to wind loading only, as expected since the wave loading does not induce twisting effects.

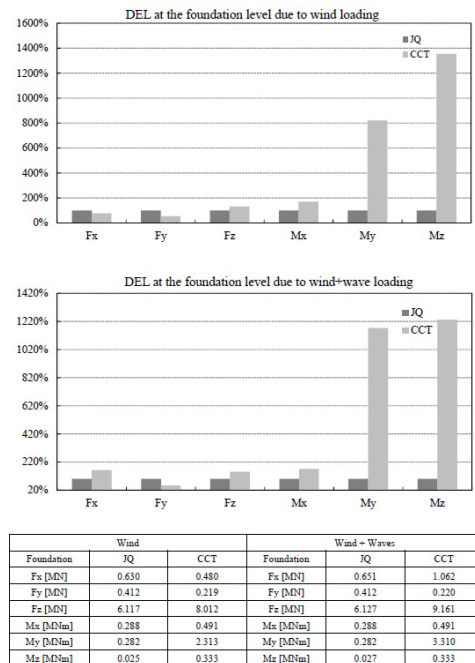


Fig. 7 Lifetime DEL at the foundation level due to wind and wind + wave loading

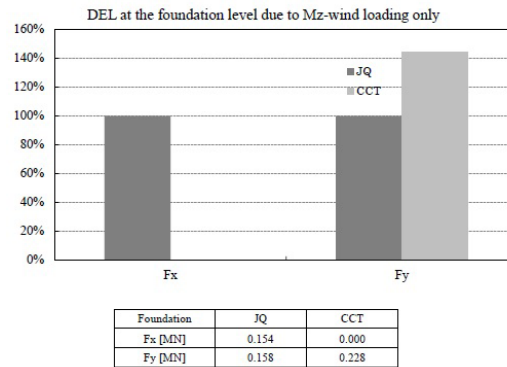


Fig. 8 Lifetime DEL at the foundation level for Mz due to wind loading

Fig. 7 shows the lifetime DELs at the foundation level for wind + wave loading, for pile n. 1' of the CCT and pile n. 1" of the JQ. The wave loading determines an increase in the Fx, My and Fz DELs, that is found much more significant in the CCT than in the JQ. This result can be explained since the structural members of the CCT feature larger diameters and, as a consequence, they undergo higher hydrodynamic forces. In this respect see Fig. 5, that shows the total wave loading on the two structures for the environmental state corresponding to $V_w = 9 \text{ ms}^{-1}$ in Table 2. On the other hand, the increase in the Fx, My and Fz DELs appears consistent with the maxima inertia forces reported in Fig. 3 and in Fig. 4: they are larger in the CCT than in the JQ and, also, the increase with respect to the corresponding ones due to wind loading only is more significant in the CCT than in the JQ. Finally, as expected no differences are encountered in the Fy and Mx DELs, since the total wave loading has no components in the y-direction. The same can be stated for the Mz DEL, since the wave loading does not induce twisting effects.

6. Conclusions

A comparative fatigue analysis has been carried out on typical CCT and JQ for OWECs, located in a reference site in the North Atlantic Ocean. Fatigue behavior has been assessed in the time domain under combined stochastic wind and wave loading. A lifetime DEL has been computed, which accounts for different load cases in a statistical framework, based on the related probabilities of occurrence. The most relevant result found for design purposes is that the DELs are generally larger in the CCT than in the JQ, both at the tower base and at the foundation level. This result is attributed mainly to: (i) the larger inertia forces in the CCT, due essentially to its larger mass, (ii) the larger hydrodynamic loads on the CCT, due to the larger diameters of its structural members and the presence of a submerged part of the tower. Due to the combination of these two effects, especially the My DEL has been found very significant at the tower base of the CCT, as compared to the corresponding one at the tower base of the JQ.

Although the conclusions of this paper have been drawn from two specific examples of CCT and JQ, in the authors' opinion similar conclusions may be expected in CCTs where masses and diameters are significantly larger than in JQs. It is evident, however, that appropriate numerical

checks should always be made for the specific CCT and JQ under consideration.

It has to be noted that the presented findings rely on a certain amount of simplifications, namely: hydrodynamic and aerodynamic loading have been generated separately and applied on a linear structural model, where additional aerodynamic damping is included to account for the coupling between aerodynamic and hydrodynamic responses; pile-soil interaction has been modeled as linear; lumped environmental load cases have been considered. These simplifications have been validated by comparison with experimental data and are certainly appropriate for a preliminary design (Van der Tempel 2006), but for the final design a fully integrated nonlinear time domain simulation is currently recommended as the most suitable tool. As a final remark, it is reminded that a definitive choice between CCT and JQ cannot ignore economic and logistic issues, generally dependent on the specific location of the wind farm (Lozano *et al.* 2011, Daim *et al.* 2012). All these aspects have not been considered in this paper and are left for further investigations.

References

- AlHamaydeh, M. and Hussain, S. (2011), "Optimized frequency-based foundation design for wind turbine towers utilizing soil-structure interaction", *J. Frankln. I.*, **348**(7), 1470-1487.
- Andersen, U.V. (2008), *Load reduction of support structures of offshore wind turbines*, Master thesis, Danish Technical University (DTU), Copenhagen.
- API RP 2A-WSD 21st edition, December 2000.
- Boccotti, P., Arena, F., Fiamma, V. and Barbaro, G. (2012), "Field experiment on random-wave forces on vertical cylinders", *Probabilist. Eng. Mech.*, **28**, 39-51.
- Boccotti, P., Arena, F., Fiamma, V. and Romolo, A. (2013), "Two small-scale field experiments on the effectiveness of Morison's equation", *Ocean Eng.*, **57**(1), 141-149.
- Camp, T.R. *et al.* (2003), *Design methods for offshore wind turbines at exposed sites*, EU Joule III Project JOR3-CT98-0284, Final Report.
- Chakrabarti, S.K. (1987), *Hydrodynamics of offshore structures*, WIT Press, Boston, USA.
- Computers and Structures (CSI) (2010), SAP2000, Berkeley, USA.
- Daim, T.U., Bayraktaroglu, E., Estep, J., Lim, D.J., Upadhyay, J. and Yang, J. (2012), "Optimizing the NW off-shore wind turbine design", *Math.Comput. Model.*, **55**(3-4), 396-404.
- Di Paola, M. and Failla, G. (2002), "Stochastic response of offshore structures by a new approach to statistical cubicization", *J. Offshore Mech. Arct. Eng.*, **124**, 6-13.
- DNV-RP-C205 (2010), *Environmental conditions and environmental loads*, Det Norske Veritas.
- De Vries, W. (2011), "UpWind_WP4_D4.2.8_Final Report WP4.2: Support structure concepts for deep water", *UpWind deliverable D4.2.8*, March 2011.
- Dong, W., Moan, T. and Gao, Z. (2011), "Long-term fatigue analysis of multi-planar tubular joints for jacket-type offshore wind turbine in time domain", *Eng.Struct.*, **33**(6), 2002-2014.
- Dong, W., Moan, T. and Gao, Z. (2012), "Fatigue reliability analysis of the jacket support structure for offshore wind turbine considering the effect of corrosion and inspection", *Reliab. Eng. Syst. Safe.*, **106**, 11-27.
- Elshafey, A.A., Haddara, M.R. and Marzouk, H. (2009), "Dynamic response of offshore jacket structures under random loads", *Mar.Struct.*, **22**(3), 504-521.
- Garrad, H. and Partners (2009), *Bladed for Windows*, Bristol, UK.
- Hansen, M.O.L. (2008), *Aerodynamics of wind turbines*, 2ndEd., Earthscan, London, UK.
- Hasselmann, K., Barnett, T.P., Bouws, E., Carlson, H. *et al.* (1973). "Measurements of wind wave growth and swell decay during the Joint North Sea Wave Project (JONSWAP)", *Deut. Hydrogr. Zeit.*, **A8**, 1-95.
- Homepage, "Alpha Ventus": <http://www.alpha-ventus.de>.

- Homepage, "Beatrice Windfarm Demonstrator Project": <http://www.beatricewind.co.uk>.
- Homepage, "Waveclimate.com": <http://www.waveclimate.com>.
- ISSC specialist committee V.4 (2006), "Ocean wind and wave energy utilization", *Proceedings of the International Ship and Offshore Structures Congress*, Southampton, U.K., 20-25 August.
- Jonkman, J., Butterfield, S., Musial, W. and Scott, G. (2009), *Definition of a 5-MW reference wind turbine for offshore system development*, Technical Report NREL/TP-500-38060, National Renewable Energy Laboratory (NREL).
- Jonkman, J. and Musial, W. (2010), *Offshore Code Comparison Collaboration (OC3) for IEA Task 23 Offshore Wind Technology and Deployment*, Technical Report NREL/TP-5000-48191, December 2010.
- Kuhn, M. (2001), *Dynamics and design optimisation of offshore wind energy conversion systems*, Report no. 2001.002, Delft University Wind Energy Research Institute (DUWIND).
- Longuet-Higgins, M.S. (1963), "The effects of non-linearities on statistical distributions in the theory of sea waves", *J. Fluid Mech.*, **17**(3), 459-480.
- Lozano-Minguez, E., Kolios, A.J. and Brennan, F.P. (2011), "Multi-criteria assessment of offshore wind turbine support structures", *Renew. Energ.*, **36**(11), 2831-2837.
- Manwell, J.F., McGowan, J.G. and Rogers, A.L. (2010), *Wind energy explained: theory, design and application*, 2nd Ed., Chichester: John Wiley & Sons.
- Matsuiski, M. and Endo, T. (1969), *Fatigue of metals subjected to varying stress*, Japan Soc. Mech., England.
- Petrini, F., Li, H. and Bontempi, F. (2010), "Basis of design and numerical modeling of offshore wind turbines", *Struct. Eng. Mech.*, **36**(5), 599-624.
- Phillips, O.M. (1967), "The theory of wind generated waves", *Adv. Hydrosci.*, **4**, 119-149.
- Sarpkaya, T. and Isaacson, M. (1981), *Mechanics of wave forces on offshore structures*, Van Nostrand Reinhold Company.
- Shinozuka, M. and Deodatis, G. (1988), "Stochastic process models for earthquake ground motion", *Probabilist. Eng. Mech.*, **3**(3), 114-123.
- Song, H., Robertson, A., Jonkman, J. and Sewell, D. (2012), "Incorporation of multi-member substructure capabilities in FAST for analysis of offshore wind turbines", *Proceedings of the Offshore Technology Conference*, Houston, Texas, April 30 - May 3.
- Song, H., Damiani, R., Robertson, A. and Jonkman, J. (2013), "A new structural dynamics module for offshore multimember substructure within the wind turbine computer-aided engineering tool fast", *Proceedings of the 23rd International Ocean, Offshore and Polar Engineering Conference (ISOPE)*, Anchorage, Alaska, June 30-July 5.
- Spanos, P.D. and Zeldin, B.A. (1998), "Monte Carlo treatment of random fields: A broad perspective", *Appl. Mech. Rev.*, **51**(3).
- Subroto, H., Narold, R., van Gilst, R., Kooijman, H.J. and Peeringa, J.M. (2006), "Bottom founded steel support structure for offshore wind turbines in deeper waters of North Sea", *Proceedings of the European Wind Energy Conference and Exhibition (EWEC)*, Athens, 27 February - 2 March.
- Sutherland, H.J. (1999), *On the fatigue analysis of wind turbines*, Report no. SAND99-0089, Sandia National Laboratories.
- Thomsen, K. (1998), *The statistical variation of wind turbine fatigue loads*, Report Risø-R-1063(EN), Risø National Laboratory, Denmark.
- Van der Tempel, J. (2006), *Design of support structures for offshore wind turbines*, Report no. 2006.029, Delft University Wind Energy Research Institute (DUWIND).
- Van der Tempel, J. and Molenaar, D.P. (2002), "Wind turbine structural dynamics - A review of the principles for modern power generation, onshore and offshore", *Wind Eng.*, **26**(4), 211-220.
- Zaaijer, M.B. (2006), "Foundation modelling to assess dynamic behaviour of offshore wind turbines", *Appl. Ocean Res.*, **28**(1), 45-57.
- Zaaijer, M.B. (2009), "Review of knowledge development for the design of offshore wind energy technology", *Wind Energy*, **12**(5), 411-430.

Appendix

Fig. 1 of this Appendix shows the two test structures and the geometry of the pertinent structural members. The following parameters have been adopted for the constructional steel: Young modulus $E = 210 \text{ GPa}$, $\nu = 0.3$.

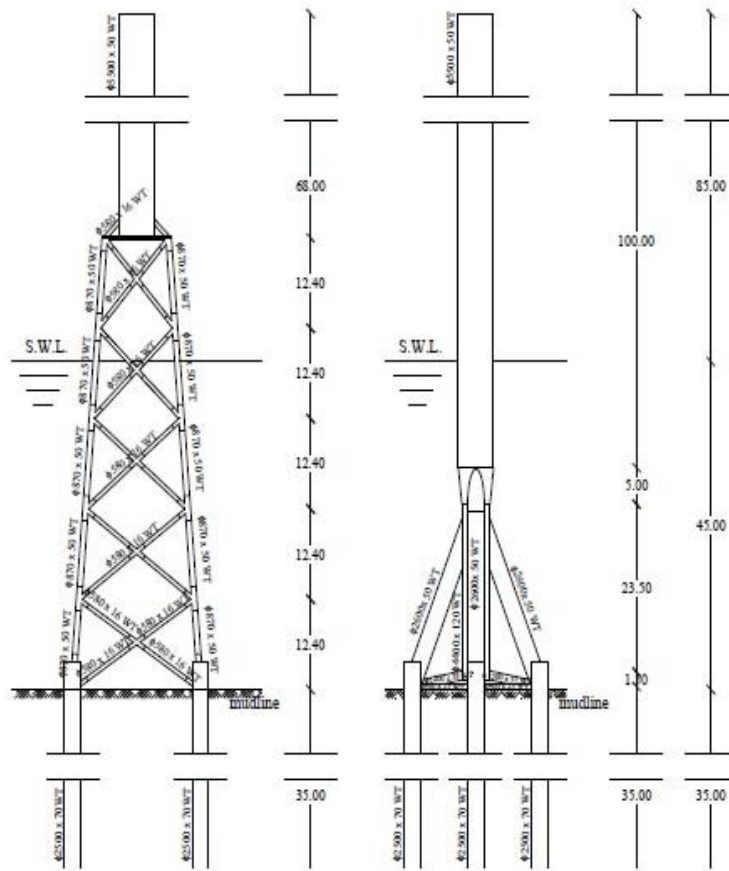


Fig.1 (Appendix) Details of the JQ and CCT (dimensions in m)